CrossMark
click for updates

Rapid surfactant-free synthesis of Mg(OH)$_2$ nanoplates and pseudomorphic dehydration to MgO†

James M. Hanlon,[a] Laura Bravo Diaz,[ab] Giulia Balducci,[a] Blane A. Stobbs,[a] Marek Bielewski,[b] Peter Chung,[c] Ian MacLaren[d] and Duncan H. Gregory*[a]

Magnesium hydroxide nanoplates *ca.* 50 nm in thickness can be prepared over minute timescales *via* hydrothermal synthesis in a multimode cavity (MMC) microwave reactor. This approach allows *ca.* 1 g of single-phase Mg(OH)$_2$ to be synthesised in less than 3 minutes without the requirement of surfactants or non-aqueous solvents. The hydroxide nanomaterial dehydrates at temperatures >200 K below that of the equivalent bulk material and can be utilised as a precursor for the pseudomorphic synthesis of nanoplates of MgO as investigated by TG-DTA-MS, PXD and SEM measurements. Equally, the pseudomorphic synthesis can be performed by irradiating the Mg(OH)$_2$ nanomaterial with microwaves for 6 minutes to produce single-phase MgO.

Introduction

Magnesium hydroxide, Mg(OH)$_2$, occurs naturally as the mineral brucite and crystallises in the trigonal space group $P\bar{3}m1$. Mg(OH)$_2$ is an important commercial material, finding widespread application as a non-toxic flame retardant and as a precursor for the synthesis of magnesium oxide, MgO.[1–4] MgO (cubic space group $Fm\bar{3}m$) is itself used for a wide variety of purposes including catalysis and toxic waste handling and used as an additive in paints and refractory materials.[5,6] Nanostructuring MgO can result in a range of improved properties compared to that of the bulk material and has resulted in MgO being used in optical materials and specifically phase plasma display technologies.[7,8] MgO is also used in various medical and pharmaceutical products, but beyond traditional uses in antacids and ointments, MgO nanoplates have recently demonstrated impressive antibacterial properties against *E. coli*.[9] Nanostructured Mg(OH)$_2$ can be produced efficiently *via* hydrothermal/solvothermal methods that involve a surfactant such as ethylenediamine (en) or polyethylene glycol (PEG), and such surfactants have been deemed

highly influential in the mechanism of nanostructure formation, acting as templates or growth inhibitors.[10] Solvothermal syntheses such as these are performed above ambient temperature and pressure and require relatively long reaction times (typically 12 h or more).

Although surfactants are commonly employed to aid in the formation of nanostructures, their inclusion ultimately adds additional cost to processing. Moreover, in many cases, use of surfactants is not environmentally sustainable. Similar concerns over environmental sustainability can be raised in cases where non-aqueous solvents are employed in solvothermal synthesis approaches. Ideally, a method that is fast, simple, and energy-efficient and removes the need for surfactants and non-aqueous solvents would represent a huge benefit. The use of microwaves (MWs) as a replacement for conventional heating approaches in both the solid state and solution-based syntheses of materials has been receiving considerable attention.[11–14] In the context of the preparation of nanostructured magnesium hydroxide, for example, nanosheets of Mg(OH)$_2$ have been synthesised in 30 minutes from MgCl$_2$, urea and NaOH using a multimode cavity (MMC) microwave reactor[15] and nanoplates of Mg(OH)$_2$ have been synthesised using MW plasma in water.[16] Using MW heating consistently decreases the reaction time dramatically compared to conventional heating methods. It was only recently that Al-Gaashani *et al.* made a significant advance in the first additive-free synthesis of Mg(OH)$_2$ using microwaves; a mixture of hydroxide nanoparticles and nanosheets was synthesised from Mg powder and water in a domestic microwave oven (DMO).[17]

Herein we present the results of synthesis experiments to prepare Mg(OH)$_2$ from readily available, inexpensive MgO

[a] WestCHEM, School of Chemistry, University of Glasgow, Glasgow, G12 8QQ, UK. E-mail: Duncan.Gregory@glasgow.ac.uk
[b] European Commission, Joint Research Centre (JRC) Institute for Energy and Transport, Westerduinweg 3, 1755 LE Petten, The Netherlands
[c] School of Geographical and Earth Sciences, Gregory Building, Lilybank Gardens, University of Glasgow, Glasgow, G12 8QQ, UK
[d] SUPA School of Physics and Astronomy, University of Glasgow, Glasgow, G12 8QQ, UK
† Electronic supplementary information (ESI) available. See DOI: 10.1039/c5ce00595g

and water by a facile, MW hydrothermal route. The method produces hexagonal nanoplates of single-phase hydroxide in less than 3 minutes without the requirement of surfactants or templating agents. Furthermore, the resulting hydroxide can be converted in a pseudomorphic reaction back to the corresponding oxide *via* a dehydration process that occurs at a temperature *ca.* 200 K below that of the dehydration temperature for bulk $Mg(OH)_2$. This pseudomorphic dehydration process can also be induced by MW heating over minute timescales.

Experimental

Synthesis

In a typical synthesis procedure, $Mg(OH)_2$ nanoplates were prepared from 0.4 (or 0.8) g of MgO (Sigma, 98%) with deionised water in a 23 (or 45) ml Teflon-lined autoclave (Parr Microwave Acid Digestion Vessels; model numbers 4781 and 4782, respectively). The autoclave was filled up to 2/3 of the total volume, sealed and heated in an MMC reactor (Panasonic, 750 W, 2.45 GHz, or Sharp R272WM, 800 W, 2.45 GHz) for 1–6 min. Note that care must be taken to ensure that the autoclave vessel is not over-filled (*e.g.* with excess water) as this can cause a rapid pressure increase in the vessel during MW heating. Under these circumstances the reaction should be stopped and allowed to cool before reheating. Rapid pressure rises can lead to a rupture of the vessel through the release of the pressure valve, which can cause damage to the equipment.

The remainder of the preparative procedure is otherwise broadly analogous to that employed in the hydrothermal synthesis of $Mg(OH)_2$ from MgO performed *via* conventional heating.[18] The obtained fine white precipitate was washed with deionised water, centrifuged and allowed to dry in air at room temperature overnight.

Magnesium oxide (MgO) nanoplates were prepared from the synthesised $Mg(OH)_2$ using the same MMC reactor as above. 50 mg of hydroxide was added to a silica tube and heated for 6 min with SiC used as a susceptor (ESI,† Fig. S1).

Characterisation

The powder X-ray diffraction (PXD) data for the reactants and products were collected using a PANalytical X'pert Pro MPD diffractometer in a Bragg–Brentano reflection geometry between $5 \leq 2\theta/^\circ \leq 85$ for 20–30 minutes, with a step size of 0.0084° and a monochromator slit width of 10 mm. Scan times of 3 h were used to collect data suitable for Rietveld refinement.

Low-resolution scanning electron microscopy (SEM) images were obtained using a Phillips XL30 ESEM instrument working in high vacuum mode with an applied accelerating voltage of 25 kV and a working distance of 5 mm for morphology and particle size measurements. Energy dispersive X-ray spectroscopy (EDX) measurements (coupled with SEM) were performed using an Oxford Instruments X-act spectrometer. The instrument was calibrated using the INCA

EDX software with Cu as the calibration standard. High resolution scanning electron microscopy (SEM) images of $Mg(OH)_2$ were obtained using a Zeiss Sigma Variable Pressure Analytics field-emission analytical SEM with an applied voltage of 15 kV and a working distance of 6.1 mm employed. Transmission electron microscopy (TEM) was performed to image the synthesised materials and to collect selected area electron diffraction (SAED) patterns. Data were taken from samples dispersed in ethanol on a carbon film support at a 200 kV accelerating voltage using a FEI Tecnai G^2 20 microscope.

Thermal analysis (thermogravimetric–differential thermal analysis–mass spectrometry, TG-DTA-MS) was performed using a Netzsch STA 409 analyser interfaced with a Hiden HPR 20 Mass Spectrometer. The STA analyser was located within an argon-filled MBraun UniLab glove box (<0.1 ppm H_2O, 0.1 ppm O_2). Approximately 30 mg of $Mg(OH)_2$ was heated to 873 K in an alumina pan under flowing Ar at a heating rate of 5 K min^{-1} and held at 873 K for 60 min.

BET measurements were performed using a Micromeritics Gemini III Surface Area Analyser. Samples (*ca.* 0.05 g) were outgassed at 383 K in flowing N_2 prior to analysis. Helium was used as a calibrant and nitrogen as the adsorbent at 77 K.

Results and discussion

Synthesis of $Mg(OH)_2$

The experimental details and salient results for selected materials are listed in Table S2 in the ESI.† 1 g of single-phase $Mg(OH)_2$ was prepared in 6 minutes at 750 W using the MW methods described above in the Experimental section (sample **1**). By increasing the input power to 800 W, it was possible to reduce the reaction time first to 4 min (sample **2**) and then, with further optimisation, to 2 min. Samples **1** and **2** were obtained as fine white powders and identified by PXD as single-phase $Mg(OH)_2$ (PDF no. 01-083-0144) with no traces of the MgO starting material present (Fig. 1).

Initial indexing and cell parameter refinement for **1** and **2** were performed using CELLREF.[19] Subsequent Rietveld refinement against the PXD data using the GSAS/EXPGUI packages (*q.v.* ESI†) resulted in lattice parameters that are in close agreement with the literature values.[20–22] Given the non-spherical morphology and non-uniform size distribution of **1** and **2** (see below), it was not deemed appropriate to employ the Scherrer method to estimate the particle size of the synthesised $Mg(OH)_2$.

Sample **1** and sample **2** are composed of regular hexagonal nanoplates, typically with a side length of *ca.* 100–300 nm (*i.e.* diagonals of 200–600 nm) and a thickness of *ca.* 10–60 nm (Fig. 2). EDX analysis of individual hexagons yielded Mg : O elemental ratios of *ca.* 1 : 2 (38(3) at.% : 62(3) at.%) confirming the identity of the material as $Mg(OH)_2$, consistent with the PXD data. BET measurements performed on **1** and **2** revealed specific surface areas of 10.16 m^2 g^{-1} and 25.62 m^2 g^{-1} and average pore diameters of 29.18 nm and 17.53 nm, respectively. These observed differences resulting from altering the reaction time and applied MW power
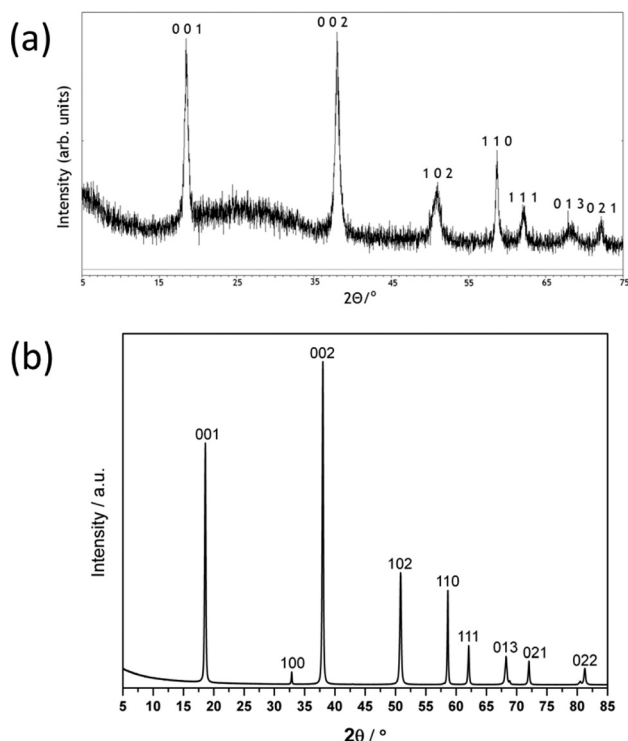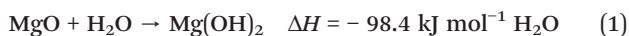
Fig. 1 PXD pattern of (a) Mg(OH)$_2$ synthesised at 750 W for 6 minutes (**1**); (b) Mg(OH)$_2$ synthesised at 800 W for 4 minutes (**2**). The *hkl* indices for the trigonal brucite phase reflections are indicated.

Fig. 2 (a) SEM micrograph of hexagonal nanoplates of Mg(OH)$_2$ at 800 W for 4 minutes (**2**); (b) SEM micrograph showing the thickness of individual nanoplates from the same sample.

prompted a detailed investigation of these experimental parameters.

Considering the 750 W MW reactions as a function of time, only after 3 min of irradiation time does any appreciable conversion of MgO to Mg(OH)$_2$ occur (Fig. 3). The reaction thereafter drives towards completion rapidly; for example, heating 0.8 g of MgO for 4 minutes produces 98 wt.% Mg(OH)$_2$ and 2 wt.% MgO (from Rietveld refinement, Table S2, ESI†). The rapid jump from negligible to almost complete conversion produces a plot that can be fit approximately to a sigmoidal curve. If the applied power is increased to 800 W then complete conversion to the hydroxide is achieved in 2 minutes. In fact, after 1 minute of heating at 800 W there is an almost negligible amount of MgO starting material present (1(2) wt.% from Rietveld Refinement). The reaction therefore proceeds simply as shown in eqn (1) with no diffraction evidence of any intermediate phases over the course of the reaction:[23,24]

$$MgO + H_2O \rightarrow Mg(OH)_2 \quad \Delta H = -98.4 \text{ kJ mol}^{-1} \text{ H}_2\text{O} \quad (1)$$

Low resolution SEM reveals that the samples prepared at intermediate irradiation times (*i.e.* prior to 100% conversion) are also composed of hexagonal nanoplates. This indicates that nanoplate growth is a rapid process. The pressure inside the vessel and the concentration of the reaction solution are undoubtedly important factors in determining the size and thickness of the Mg(OH)$_2$ nanoplates formed. Although we
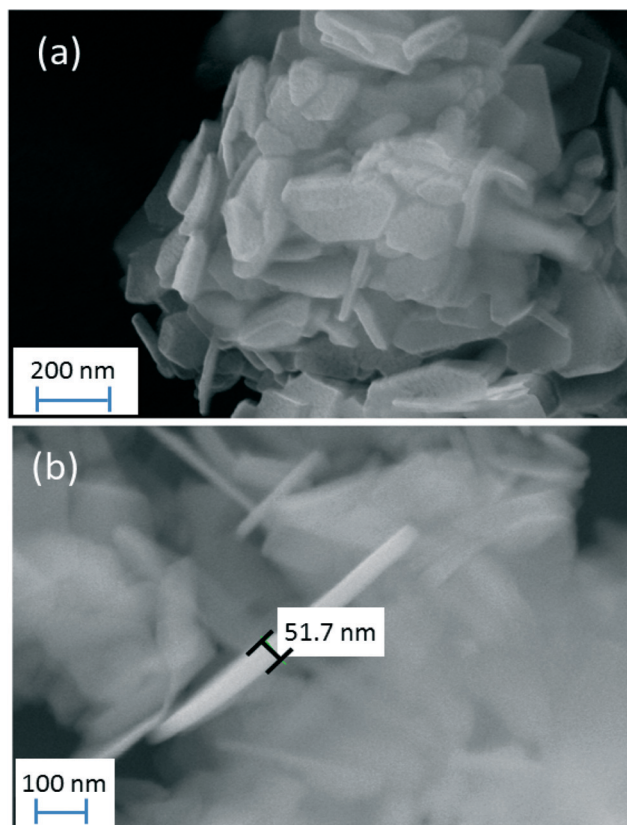
have not examined this in detail, this pressure can be affected by the MgO : H$_2$O ratio and the volume of water used in the synthesis procedure. There are reports in the literature on the effect of pressure on the morphology and particle size of the final product and, for example, the concentration of
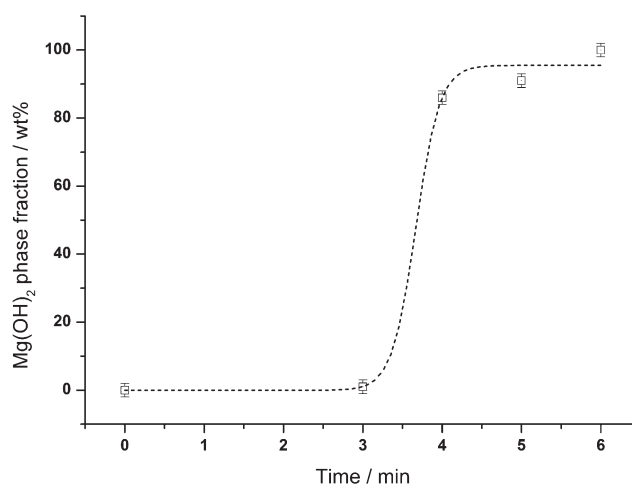

Fig. 3 Plot of Mg(OH)$_2$ phase fraction against reaction time for samples prepared at 750 W using a 23-ml autoclave. The dotted line shows a tentative sigmoidal fit to the data.

the starting materials is an important factor in the dimensions of ceria crystallites obtained by hydrothermal treatment.[25] Similarly, Ma *et al.* studied the effect of the concentration of the precursor and the synthesis pressure on the formation of Cu_2O nanostructures and found that both the concentration and pressure have profound effects on the final products (where, for example, the dimensionality develops from 0D (particles) to 1D (fibres) with increasing pressure).[26]

The TEM images of individual platelets from **2** confirm the dimensions of the particles observed by SEM, and SAED experiments demonstrate that each hexagon is single crystalline (Fig. 4). Diffraction patterns could be indexed to the trigonal $P\bar{3}m1$ structure of $Mg(OH)_2$. The flat faces of each hexagon are formed on the (0001) basal plane, and the hexagonal edges are formed on the $\{10\bar{1}0\}$ planes. The formation of the hexagonal lamellae is consistent with the higher growth rate normal to the crystallographic *c*-axis (as compared to the rate of growth parallel to *c*) previously observed in brucite.[27]
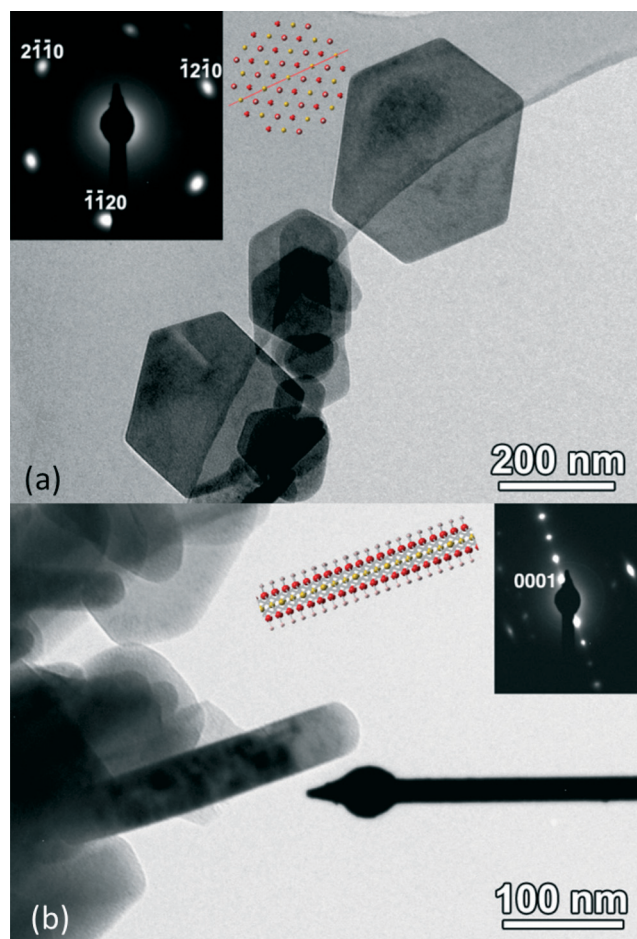

Fig. 4 TEM images and diffraction patterns showing the crystallography of the hexagonal platelets recorded (a) perpendicular to and (b) parallel to the flat faces. Ball and stick models of the crystal structure are shown for both cases. The red line in the ball and stick model denotes the $(10\bar{1}0)$ plane (yellow spheres – magnesium; red spheres – oxygen; and small grey spheres – hydrogen).

Role of templating agents in $Mg(OH)_2$ nanoparticle synthesis

In order to discuss the reasons as to how nanoplates can be synthesised solvothermally without surfactants, comparisons can be made with previously reported syntheses and the proposed mechanisms of templated $Mg(OH)_2$ nanostructure formation. Polyethylene glycol (PEG) has been successfully employed previously and the morphology of the hydroxide appears to be dependent on the PEG concentration and average molecular weight. PEG-1000 leads predominantly to 1D nanostructures, whereas Wang *et al.* employed PEG-20 000 to yield nanoplates.[10,28] In the latter case, it was postulated that Mg^{2+}–PEG pairs form in solution, which generate hexagonal pores on stirring and aging. The network of pores is proposed to evolve from the twisting and coiling of a sterically-unstable Mg^{2+}–PEG matrix. The addition of NaOH leads to the formation of $Mg(OH)_2$ crystal nuclei following reaction between the OH^- ions and the Mg^{2+} ions within the hexagonal pores. During hydrothermal synthesis, there is growth of these crystal nuclei that leads to the formation of the hexagonal nanoflakes after the removal of PEG (through washing with distilled water and ethanol). The authors state that without using a surfactant no nanostructures were observed in the product. A similar growth mechanism is proposed when ethylenediamine (en) is used as a template and either nanotubes or nanoplates can result.[4,29] The bidentate ligand complexes with Mg^{2+} and as the temperature increases in the hydrothermal reaction, the stability of the Mg–en complex decreases. OH^- ions (from H_2O) are proposed to bind to the complex leading to the loss of en, the formation of Mg–O bonds and finally the formation of the $Mg(OH)_2$ product.

In fact, a reasonable argument might be made that $Mg(OH)_2$ nanoparticle morphology is determined as much by pH as by structure-directing agents. Operating at high pH (*e.g.* by addition of NaOH) takes the reaction mixture beyond the isoelectric point for $Mg(OH)_2$ (pH ~12), creating negatively charged hydroxide surfaces to which cations (such as Na^+ in the case of NaOH) bind non-selectively. This restricts $Mg^{2+}_{(aq)}$ access to the surface and encourages isotropic growth and aggregation.[30] By contrast, addition of weaker bases (or no base addition) favours preferential binding of OH^- to the basal plane, anisotropic, edge-directed growth and hence formation of platelets. This is precisely the crystalline form of naturally-occurring brucite.[31]

Mechanism of MW-synthesised $Mg(OH)_2$ nanoplate formation

In the synthesis route described herein, we have obtained $Mg(OH)_2$ nanoplates without the addition of a templating species or base. Hence a structure-directing agent does not appear to be essential to obtain 2D nanostructures. A mechanism of nanoplate formation was proposed by Yu *et al.* for the corresponding conventionally heated hydrothermal synthesis (also using only MgO and H_2O as the reactants).[18] The first step of this process is the dissolution of bulk MgO in H_2O, which results in the formation of primary particles.

Aggregation of these primary particles occurs leading to the formation of mesoporous nanoplates. Similarly, Shah and Qurashi produced MgO nanoflakes (*via* subsequent heating of $Mg(OH)_2$) from Mg powder and distilled water only and proposed that Mg^{2+} reacts with H_2O at room temperature to form $Mg(OH)_2$ colloids.[32]

Although the $Mg(OH)_2$ particle sizes obtained from our MW synthesis route are very similar to those in the studies above, it is notable that although we observed type IV isotherms typical of mesoporous solids, the specific surface area appears to be lower. Furthermore, whereas intergranular porosity is observed, there is no visual evidence of the "wormlike" mesopores (each of *ca.* 4 nm) observed in hydroxide plates by Yu *et al.*[18] Therefore, one might expect that the mechanism for $Mg(OH)_2$ formation in the experiments described herein is not identical to that proposed previously (Fig. 5a). The BET surface area and porosity measurements for the samples prepared at 800 W (Table 1) illustrate that as the heating time is increased, the surface area first decreases and subsequently increases as the reaction proceeds to completion (≥ 2 min) before reduction, as might be expected at extended heating times (8 min). The pore diameter, however, progressively decreases with longer heating time.

Although the solubility of both MgO and $Mg(OH)_2$ is rather poor at room temperature, the values improve significantly as the temperature is increased.[33,34] The hydration of MgO is believed to occur *via* a dissolution–reprecipitation process, the mechanism of which involves the formation of $Mg(OH)_2$ at the MgO surface (*via* the $MgOH^+$ species, eqn (2)) and subsequent removal of hydroxide from the oxide surface.[35,36] MgO reacts rapidly with water and the formation of $Mg(OH)_2$ is believed to be faster than its removal from the MgO surface. In fact, very rapid hydration of MgO has previously led to relatively large hydroxide aggregates of submicron crystallites.[37]
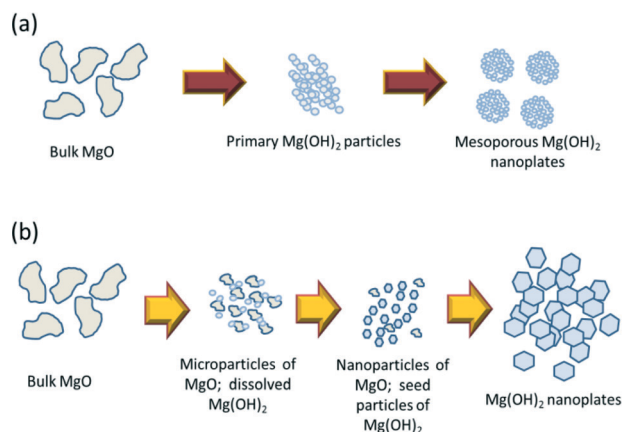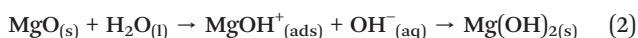
$$MgO_{(s)} + H_2O_{(l)} \rightarrow MgOH^+_{(ads)} + OH^-_{(aq)} \rightarrow Mg(OH)_{2(s)} \quad (2)$$

Fig. 5 Proposed hydration and growth processes for (a) the conventional hydrothermal synthesis of $Mg(OH)_2$ nanoplates according to Yu *et al.*;[18] (b) the additive-free microwave hydrothermal synthesis of $Mg(OH)_2$ nanoplates performed in this work.

The principal difference between MW and conventional hydrothermal synthesis lies in the rate of heating (and cooling). MWs interact with water as a polar solvent.[38] Given that the loss tangent, $\tan \delta$, which governs the ability of a substance to convert irradiated energy to heat, is high, then the temperature of the aqueous solution increases rapidly. Hence, one would expect, as in the conventional case, the MW synthesis of $Mg(OH)_2$ from MgO to proceed *via* an initial dissolution step but which in the MW case, is likely to be extremely rapid. This is reflected in the proposed sigmoidal shape of the phase fraction *vs.* time plot in Fig. 3 and the observed changes in the diffraction peak width over time. Diffraction peak widths for selected reflections (for samples irradiated at 800 W) are detailed in the ESI (Table S8, Fig. S13†). There is a general trend towards the narrowing of $Mg(OH)_2$ peaks as the heating time is increased from 2 minutes and beyond. In the first 2 minutes of irradiation at 800 W, however, there is strong evidence of peak broadening, indicative of particle size reduction, dissolution and formation of $Mg(OH)_2$ from solution. Nanoplate growth is concluded on cooling. The observed agglomeration of nanoplates, a lack of microporosity and a relatively low total pore volume in all materials indicate that the assemblage of primary particles into larger plates is unlikely to be the mechanism of growth in our MW synthesis and that these particles are likely to nucleate and grow individually and agglomerate. TEM and SAED evidence would tend to support this premise given that the hexagonal hydroxide platelets are single crystalline. A representation of the proposed mechanism for our MW synthesis is presented in Fig. 5b. This mechanism illustrates that the use of a surfactant or template (or base) is not necessary for the synthesis of $Mg(OH)_2$ nanoplates themselves, but could assist in suppressing subsequent agglomeration (and increasing the overall surface area). Equally, other factors such as the heating and cooling rate (applied MW power and irradiation time) and the initial morphology (particle size and surface area) of the MgO starting material may prove important tools in controlling agglomeration without the need for additives. These are variables that we are currently investigating further. Intriguingly, Al-Gaashani *et al.* observed two different co-existing product morphologies when magnesium metal is reacted with water to produce $Mg(OH)_2$ in a microwave field.[17] They suggested that different Mg species in solution were the origin of this morphological diversity. We see no evidence for equivalent phenomena in the hydration of MgO.

Dehydration of $Mg(OH)_2$ nanoplates

TG-DTA-MS data for 2 are shown in Fig. 6. The nanostructured $Mg(OH)_2$ begins to lose weight at 548 K and reaches a stable final mass by 678 K. The DTA curve reaches a maximum at 665 K and confirms that the reaction process is endothermic. Mass spectra confirm that water is the sole gaseous species evolved during heating and dehydration would thus be expected to proceed *via* the reverse of the reaction

Table 1 Specific surface area and porosity for MgO hydrated at 800 W as a function of irradiation time

Irradiation time (min)	Specific surface area ($m^2 g^{-1}$)	Mean pore diameter (nm)	Phase composition[a]
0	2.87(8)	30.7	MgO
1	27.5(1)	28.5	MgO; Mg(OH)$_2$
2	10.3(1)	25.8	Mg(OH)$_2$
3	20.5(3)	25.0	Mg(OH)$_2$
4	25.6(2)	17.5	Mg(OH)$_2$[b]
8	17.3(2)	14.1	Mg(OH)$_2$

[a] From Rietveld refinement against the PXD data. [b] Sample 2.

given by eqn (1). It has been previously reported that when the particle size of Mg(OH)$_2$ is decreased to the nanoscale level (25–200 nm), then the decomposition temperature can be reduced by over 200 K to 553–603 K (as measured by TGA performed under flowing N$_2$).[4] A similar reduction in dehydration temperature occurs for our material (2) where loss of water occurs between 548 K and 678 K from the TG curve corresponding to a mass reduction of 29.40 wt.%. These values are compared to a theoretical weight loss of 30.9 wt.% for the dehydration of Mg(OH)$_2$.

PXD of the samples following TG-DTA-MS measurements revealed single-phase MgO (PDF card 01-071-6488, Fig. 7) as the only solid crystalline product. Given that the weight loss

is 95.1% of the calculated value for Mg(OH)$_2$ dehydration, it is reasonable to assume that any amorphous product is also likely to be MgO. The lattice parameter obtained from Rietveld refinement for the obtained MgO is 4.220(3) Å, which is comparable to the literature value of 4.214(1) Å.[39] The refinement data for the obtained MgO (3) are presented in the ESI.†

SEM images of 3 (Fig. 8) show dense clusters of hexagonal platelets verifying that the morphology of the hydroxide is retained following heating and that the decomposition from Mg(OH)$_2$ is pseudomorphic. High magnification micrographs demonstrate that the hexagonal diagonal dimension of the nanoplates is similar to that of the Mg(OH)$_2$ material before dehydration (typically 200–300 nm) with thicknesses of approximately 10–40 nm. EDX experiments yielded 1:1 Mg:O elemental ratios (56(2) at.%:44(2) at.%). BET measurements performed on 3 show a decrease in BET surface area from 25.6 $m^2 g^{-1}$ to 19.9 $m^2 g^{-1}$. However, the average pore diameter of the MgO is 26.9 nm, which is larger than that of 2. As with the hydroxide nanoplates, the porosity of the materials would appear to originate principally from the agglomeration of the plates and as individual nanoplates grow (decrease in surface area) the size of the voids between particles increases. By analogy with conventional hydrothermally grown Mg(OH)$_2$ (ref. 30), over prolonged heating periods (≫4 min), one would expect Mg(OH)$_2$, and therefore MgO formed from pseudomorphic dehydration, to decrease in surface area with a concomitant decrease in total pore volume.

Dehydration of 2 was also performed in the MMC with SiC used as a MW susceptor. A fine powder of single-phase MgO (4) was obtained following 6 min of irradiation. The lattice parameter obtained from Rietveld refinement for 4 is 4.219(2) Å (ESI†), which is again in good agreement with the literature value[39] and consistent with the dehydrated sample obtained by conventional heating (i.e. from TG-DTA, 3). The SEM micrographs of 4 demonstrated that the morphology of
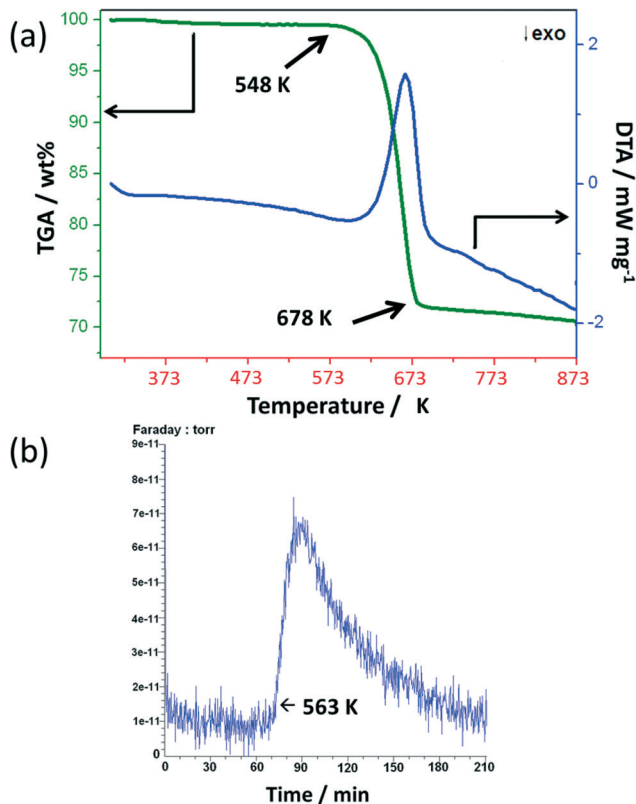

Fig. 6 (a) TG-DTA profile for 2 heated in air to 873 K; (b) corresponding MS profile for water (m/z = 18), showing a dehydration onset temperature of 563 K.
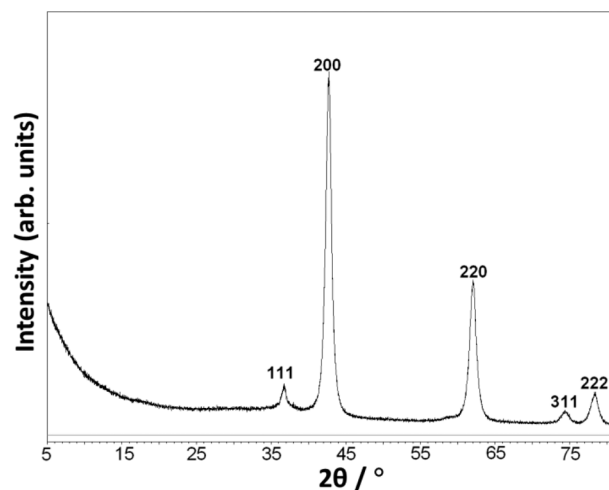

Fig. 7 PXD pattern of the dehydration product (3) from Mg(OH)$_2$ (2). The indices of the Bragg reflections corresponding to cubic MgO are indicated.
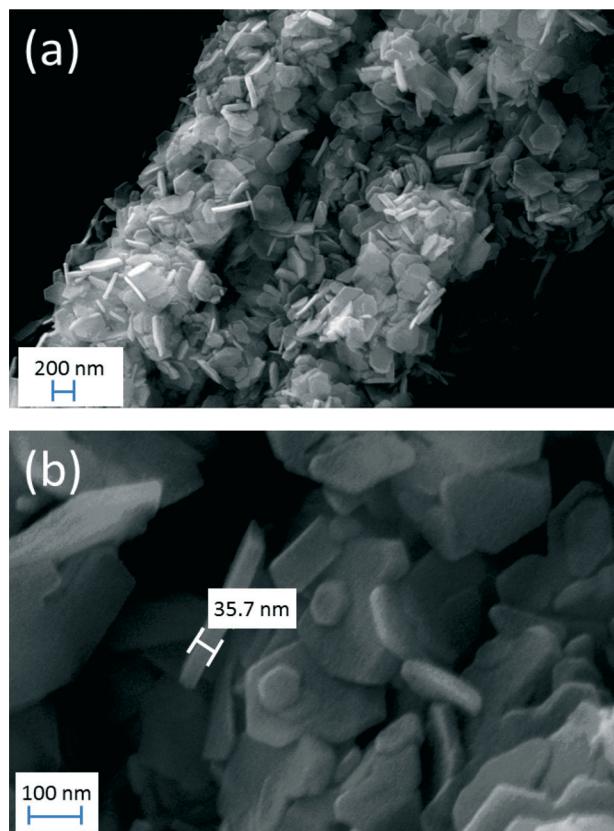
Fig. 8 (a) SEM micrograph of the hexagonal nanoplates of MgO (**3**); (b) SEM micrograph showing the thickness of the individual nanoplates from the same sample.

the synthesised $Mg(OH)_2$ (**2**) is retained after MW heating (ESI,† Fig. S13) and hence similar to the dehydration of $Mg(OH)_2$ by conventional heating, the process is pseudomorphic. **4** consists of platelets varying between 200–300 nm across and 30–50 nm in thickness. EDX analysis of the platelets yielded a 1:1 Mg:O elemental ratio (53(3) at.%:47(3) at.%). The BET surface area of **4** was measured as 22.9(7) $m^2\ g^{-1}$ with an average pore diameter of 19.1 nm. Hence, the microwave-driven dehydration achieves effectively the same result as that obtained from conventional heating and it is thus possible to convert from bulk MgO through nanostructured $Mg(OH)_2$ to nanostructured phase-pure MgO in a total processing time of 10 min or less. As with the hydroxide nanoplates (**2**), the porosity of the materials would appear to originate principally from the agglomeration of the plates, and as individual nanoplates grow (decrease in surface area), the size of the voids between particles increases.

With respect to the MW–dehydrogenation therefore, the length of irradiation time becomes as important in the solid state reaction as it is in the hydrothermal synthesis of $Mg(OH)_2$. The selection of MW-susceptor is also important since a very rapid increase in temperature greater than 1273 K (such as is often achieved by using carbon)[11] would likely lead to sintering of MgO and a decrease in surface area. Iron wool has previously been found to be effective in assisting

the formation of nanocubes of MgO *via* rapid (*ca.* 30 s) MW oxidation of Mg pieces.[39] In the work discussed herein, SiC appears to be an appropriate choice in terms of reaching the temperature regime required for dehydration, as indicated by TGA-DTA-MS, without inducing sintering. The influence of irradiation power, irradiation time and susceptor selection on the temperature and mechanism of the MW-dehydration of $Mg(OH)_2$ will be the subject of further study.

Conclusions

In summary, we have synthesised single-phase hexagonal nanoplates of $Mg(OH)_2$ in an MMC MW reactor from MgO and H_2O. This synthetic route allows gram-scale quantities of materials to be synthesised very rapidly and energy-efficiently compared to conventional hydrothermal synthesis and requires no surfactants. The as-produced nanostructured $Mg(OH)_2$ decomposes endothermically between 548 and 678 K evolving only water and yielding MgO as the sole crystalline solid product (amassing to 29.40%, *ca.* 95% of the expected theoretical weight loss for dehydration). The phase-pure dehydration product, MgO, can be obtained by either conventional or microwave heating, with the latter achieved after only 6 minutes. The oxide retains the nanostructure of the hydroxide and hence the dehydration is pseudomorphic. These results demonstrate that $Mg(OH)_2$ produced *via* MW synthesis can be used as an effective precursor for nanostructured MgO, which in turn can be synthesised rapidly *via* microwave heating.

Acknowledgements

Notes and references

1 L. Zhuo, J. Ge, L. Cao and B. Tang, *Cryst. Growth Des.*, 2009, **9**, 1.
2 W. Wang, X. Qiao, J. Chen and H. Li, *Mater. Lett.*, 2007, **145**, 3218.
3 D. Jin, X. Gu, X. Yu, G. Ding, H. Zhu and K. Yao, *Mater. Chem. Phys.*, 2001, **112**, 968.
4 Y. Ding, G. Zhang, H. Wu, B. Hai, L. Wang and Y. Qian, *Chem. Mater.*, 2001, **13**, 435.
5 M. A. Aramendia, V. Borau, C. Jimenez, J. M. Marinas, A. Porras and F. J. Urbano, *J. Catal.*, 1996, **161**, 829.
6 M. D. D. Garcia-Sato and E. M. Camacho, *Sep. Purif. Technol.*, 2006, **48**, 36.
7 A. Kumor and J. Kumor, *J. Phys. Chem. Solids*, 2008, **67**, 2764.

8   N. C. S. Selvam, R. T. Kumar, L. J. Kennedy and J. J. Vijaya, *J. Alloys Compd.*, 2011, **509**, 9809.

9   F. Luo, J. Lu, W. Wang, F. Tan and X. Qiao, *Micro Nano Lett.*, 2013, **8**, 479.

10 Q. Wang, C. Li, M. Guo, L. Sun and C. Hu, *Mater. Res. Bull.*, 2014, **51**, 35.

11 H. J. Kitchen, S. R. Vallance, J. L. Kennedy, N. Tapia-Ruiz, L. Carassiti, A. Harrison, A. G. Whittaker, T. D. Drysdale, S. W. Kingman and D. H. Gregory, *Chem. Rev.*, 2014, **114**, 1170.

12 K. L. Harrison and A. Manthiram, *Chem. Mater.*, 2013, **25**, 1751.

13 M. Baghbanzadeh, L. Carbone, P. D. Cozzoli and C. O. Kappe, *Angew. Chem., Int. Ed.*, 2011, **50**, 11312.

14 Y. J. Zhu and F. Chen, *Chem. Rev.*, 2014, **114**, 6462.

15 F. A-Hazmi, A. Umar, G. N. Dar, A. A. Al-Ghamdi, S. A. Al-Sayari, A. Al-Hajry, S. H. Kim, R. M. Al-Tuwirqi, F. Alnowaiserb and F. El-Tantawy, *J. Alloys Compd.*, 2012, **519**, 4.

16 Y. Hattori, S. Mukasa, H. Toyota, T. Inoue and S. Nomura, *Mater. Chem. Phys.*, 2011, **131**, 425.

17 R. Al-Gaashani, S. Radiman, Y. Al-Douri, N. Tabet and A. R. Daud, *J. Alloys Compd.*, 2012, **521**, 71.

18 J. C. Yu, A. Xu, L. Zhang, R. Song and L. Wu, *J. Phys. Chem. B*, 2004, **108**, 64.

19 J. Laugier and B. Bochu, *"CELREF Unit-Cell Refinement Software on a Multiphase System"*, Laboratoire des Materiaux et du Genie Physique Ecole Nationale Suprieure de Physique de Grenoble.

20 B. H. Toby, *J. Appl. Crystallogr.*, 2001, **34**, 210.

21 A. C. Larson and R. B. von Dreele, *The General Structure Analysis System, Los Alamos National Laboratories, Report LAUR 086–748*, LANL, Los Alamos, NM, 2000.

22 V. Kazimirov, M. B. Smirnov, L. Bourgeios, L. Guerlou Demourgues, L. Servant, A. M. Balagurov, I. Natkaneic, N. R. Khasanova and E. V. Antipov, *Solid State Ionics*, 2010, **181**, 1764.

23 B. V. L'vov, A. V. Novchikhin and A. O. Dyakov, *Thermochim. Acta*, 1998, **315**, 135.

24 F. Leardini, J. R. Area, J. Bodega, J. F. Fernández, I. J. Ferrer and C. Sánchez, *Phys. Chem. Chem. Phys.*, 2010, **12**, 572.

25 A. B. Corradi, F. Bondioli, A. M. Ferrari and T. Manfredini, *Mater. Res. Bull.*, 2006, **41**, 38.

26 D. Ma, H. Liu, H. Yang, W. Fu, Y. Zhang, M. Yuan, P. Sun and X. Zhou, *Mater. Chem. Phys.*, 2009, **116**, 458.

27 K. Nakamura, S. Hirano and S. Somlya, *J. Am. Ceram. Soc.*, 1975, **58**, 349.

28 J. Zheng and W. Zhou, *Mater. Lett.*, 2014, **127**, 17.

29 Y. Li, M. Sui, Y. Ding, G. Zhang, J. Zhuang and C. Wang, *Adv. Mater.*, 2000, **22**, 818.

30 C. Henrist, J.-P. Mathieu, C. Vogels, A. Rulmont and R. Cloots, *J. Cryst. Growth*, 2003, **249**, 321.

31 G. W. Brindley and G. J. Ogilvie, *Acta Crystallogr.*, 1952, **5**, 412.

32 M. A. Shah and A. Qurashi, *J. Alloys Compd.*, 2009, **482**, 548.

33 H. Remy and A. Kuhlmann, *Z. Anal. Chem.*, 1924, **65**, 1.

34 J. K. Gjaldbaek, *Z. Anorg. Allg. Chem.*, 1925, **144**, 269.

35 G. L. Smithson and N. N. Bakhshi, *Can. J. Chem. Eng.*, 1969, **47**, 508.

36 S. D. F. Rocha, M. B. Mansur and V. S. T. Ciminelli, *J. Chem. Technol. Biotechnol.*, 2004, **79**, 816.

37 D. Filippou, N. Katiforis, N. Papassiopi and K. Adam, *J. Chem. Technol. Biotechnol.*, 1999, **74**, 322.

38 C. Gabriel, S. Gabriel, E. H. Grant, B. S. J. Halstead and D. M. P. Mingos, *Chem. Soc. Rev.*, 1998, **27**, 213.

39 (*a*) V. G. Tsirel'son, A. S. Avilov, Y. A. Abramov, E. L. Belokoneva, R. Kitaneh and D. Feil, *Acta Crystallogr., Sect. B: Struct. Sci.*, 1998, **54**, 8; (*b*) N. Takahashi, *Solid State Sci.*, 2007, **9**, 722.